

## Original Article

# Evaluation of $^{18}\text{F}$ -FAPI-42-RGD as a novel dual-targeting PET tracer in gastric cancer xenograft models

Yongsheng Zhao<sup>1,2</sup>, Jun Li<sup>2</sup>, Ping Chen<sup>3</sup>, Zhan Li<sup>2</sup>, Yongqiang Yu<sup>4</sup>

<sup>1</sup>Department of Nuclear Medicine, The First Affiliated Hospital of Anhui Medical University, Hefei, Anhui, China; <sup>2</sup>Department of Nuclear Medicine, Peking University Shenzhen Hospital, Shenzhen, Guangdong, China; <sup>3</sup>Department of Pharmacy, Peking University Shenzhen Hospital, Shenzhen, Guangdong, China; <sup>4</sup>Department of Radiology, The First Affiliated Hospital of Anhui Medical University, Hefei, Anhui, China

Received February 9, 2025; Accepted March 7, 2025; Epub April 15, 2025; Published April 30, 2025

**Abstract:** Objective: The heterogeneity of gastric cancer (GC) poses significant challenges for the detection capabilities of monomeric fibroblast activation protein inhibitor (FAPI) tracers, particularly in cases with low FAP expression. To address this limitation, a dual-target heterodimeric radiotracer,  $^{18}\text{F}$ -FAPI-42-RGD, was designed to target both FAP and integrin  $\alpha\text{v}\beta\text{3}$ . This study aimed to evaluate the efficacy of  $^{18}\text{F}$ -FAPI-42-RGD in GC models and compare its performance with the mono-specific radiotracer,  $^{18}\text{F}$ -FAPI-42. Methods:  $^{18}\text{F}$ -FAPI-42-RGD was synthesized, and its radiochemical properties and stability were assessed. Micro-PET imaging and biodistribution studies were conducted in BALB/C nude mice bearing MKN-45, N87-18.2, NUGC4 tumors, and GC patient-derived xenografts (PDX). The results were compared with those obtained from  $^{18}\text{F}$ -FAPI-42. Results:  $^{18}\text{F}$ -FAPI-42-RGD demonstrated excellent stability in saline and fetal bovine serum (FBS) for at least 2 hours. Compared to  $^{18}\text{F}$ -FAPI-42,  $^{18}\text{F}$ -FAPI-42-RGD exhibited significantly enhanced tumor uptake in MKN-45, N87-18.2, NUGC4, and GC-PDX tumors at all time points. Biodistribution studies revealed that  $^{18}\text{F}$ -FAPI-42-RGD had markedly higher tumor uptake in GC models compared to  $^{18}\text{F}$ -FAPI-42, particularly in the MKN-45, N87-18.2, and GC-PDX tumor models. The uptake of  $^{18}\text{F}$ -FAPI-42-RGD in these tumors was significantly greater than that of  $^{18}\text{F}$ -FAPI-42 ( $4.97 \pm 1.36$  vs.  $2.18 \pm 1.26$ ,  $7.02 \pm 0.97$  vs.  $2.34 \pm 0.11$ , and  $4.49 \pm 1.29$  vs.  $1.09 \pm 0.46$  %ID/g in MKN-45, N87-18.2, and GC-PDX, respectively, at 4 h post-injection). Conclusion: The dual-targeting PET tracer  $^{18}\text{F}$ -FAPI-42-RGD demonstrated significantly enhanced tumor uptake in GC models, along with a clearer background compared to  $^{18}\text{F}$ -FAPI-42. This indicates its superior diagnostic performance, suggesting its potential for clinical translation in the imaging and diagnosis of GC.

**Keywords:**  $^{18}\text{F}$ -FAPI-42-RGD, fibroblast activation protein, integrin  $\alpha\text{v}\beta\text{3}$ , gastric cancer, PET imaging, dual-targeting tracer

## Introduction

Gastric cancer (GC) is one of the most common malignant tumors worldwide, with its incidence and mortality ranking fifth and fourth, respectively, among all cancers [1]. Early detection, accurate diagnosis, and staging are critical for effective patient management and have a significant impact on prognosis. Currently, 2-[ $^{18}\text{F}$ ]fluorodeoxyglucose ( $^{18}\text{F}$ -FDG) positron emission tomography/computed tomography (PET/CT) is the dominant method for detecting malignancies [2]. However, the detection rate of GC by  $^{18}\text{F}$ -FDG PET/CT is influenced by the pathological type of tumor and the amount of FDG uptake in the gastric wall, leading to suboptimal sensitivity [3]. Therefore, there is an urgent need for more accurate and reliable early diagnostic tools, which has inspired the development of new alternative PET tracers for GC patients.

Fibroblast activation protein (FAP) is a member of the type II transmembrane serine protease family and is highly expressed in the stroma of more than 90% of epithelial cancers [4]. In contrast, its expression in normal organs and tissues is very limited. FAP overexpression is closely associated with cancer-associated fibroblasts (CAFs), which are specialized cells present in the tumor micro-

environment [5]. Due to its specific localization on CAFs, FAP has emerged as an attractive target for cancer diagnosis and therapy [6, 7]. To date, fibroblast activation protein inhibitors (FAPIs) have shown great potential as PET tracers, with significant improvements in tumor uptake, sensitivity, tumor-to-background ratio (T/B), and overall tumor detection rate [8]. Several FAPI monomers, such as FAPI-02, FAPI-42, and FAPI-46, along with other tracers targeting FAP, like the cyclic peptide FAP-2286, have been developed and evaluated for their potential in theranostic applications. While monomeric FAPI tracers have shown effectiveness over  $^{18}\text{F}$ -FDG in specific cases, issues such as limited detection capability in cancers with low FAP expression and rapid elimination hinder their broader utilization [9-11].

Integrin  $\alpha\text{v}\beta\text{3}$  is another crucial protein biomarker that plays a significant role in tumor imaging and therapy. It is highly expressed in activated endothelial cells during tumor angiogenesis and is involved in various cancer-related processes, including cell adhesion, migration, and survival [12]. An  $\alpha\text{v}\beta\text{3}$  integrin-conjugated radiotracer based on the Arg-Gly-Asp (RGD) sequence has been developed for the detection of lesions and angiogenesis. This tracer has been used in the diagnosis and staging of vari-

ous cancers, including GC, breast cancer, glioma, and lung cancer [13, 14].

The diverse tumor heterogeneity observed in various types of cancer results in poor absorption of tracers that target only one specific aspect. To address the shortcomings of single-target tracers, novel designs have been developed. These new approaches, such as heterodimers that bind to multiple targets within a single entity, aim to improve detection accuracy [15, 16]. A heterodimeric peptide, known as FAPI-RGD, was recently created by combining FAPI-02 and cyclo-RGD-D-Phe-Lys (c[RGDfK]) to target both FAP and integrin  $\alpha v \beta 3$  receptors [17-19]. In mouse xenografts, the uptake and retention of <sup>68</sup>Ga-FAPI-02-RGD were markedly higher compared to <sup>68</sup>Ga-FAPI-02 and <sup>68</sup>Ga-c(RGDfK) [20]. However, the diagnostic performance of <sup>18</sup>F-FAPI-42-RGD PET in GC remains unclear.

The aim of this study is to investigate <sup>18</sup>F-FAPI-42-RGD as a novel dual-targeting PET radiotracer, assessing its accumulation in GC xenografts and contrasting it with the mono-specific radiotracer, <sup>18</sup>F-FAPI-42.

## Materials and methods

### Patients

Specimens of GC were selected from patients who underwent gastric surgical resection between January 2023 and December 2023 at the Department of Gastrointestinal Surgery, Peking University Shenzhen Hospital. Inclusion criteria included patients diagnosed with gastric adenocarcinoma who underwent radical gastrectomy with or without postoperative therapy. All patients were followed up every 3 months. The study was conducted in accordance with the Declaration of Helsinki and was approved by the Ethics Committee of Peking University Shenzhen Hospital.

### Immunohistochemistry of human tissue samples

Immunohistochemistry (IHC) was conducted on tumor-induced gastric lesions obtained from patients with GC. Tissue sections were stained with FAP antibody (ab53066, Abcam) and integrin  $\alpha v$  antibody (GB11293-2-100, Servicebio). To neutralize endogenous peroxidase, slides were microwaved three times for 5-10 minutes and treated with 3% hydrogen peroxidase for 15 minutes at room temperature. Primary antibodies were applied overnight at 4°C. A secondary anti-rabbit or anti-mouse HRP-conjugated antibody was then incubated for 50 minutes at room temperature. Visualization was done with 3,3'-diaminobenzidine for 5 minutes and counterstained with Mayer's hematoxylin for 15 minutes, followed by washing in distilled water.

The expression levels of FAP and integrin  $\alpha v$  were assessed using the H-score method [21]. Weak immunodensity staining was assigned a score of 1, moderate

immunoreactivity was given a score of 2, and strong immunostaining intensity corresponded to a score of 3. The overall H-score was calculated by multiplying the percentage of tumor cells exhibiting each staining density by the associated numeric score for staining intensity and summing these values.

### Reagents, cell culture, and tumor models

The precursor (NOTA-FAPI-42-RGD) was obtained from Nanchang Tanzhen Biotechnology Co., Ltd. The human GC cell lines MKN-45 and NUGC4 were obtained from Cellverse Co., Ltd., while the NCI-N87-Claudin18.2 cell line was purchased from Sanyou Biopharmaceutical Co., Ltd. The NCI-N87-Claudin18.2 cell line, noted for its high expression of Claudin18.2, is referred to as N87-18.2. Tumor models were established by preparing the cells following standard protocols. Animal experimental procedures and protocols were approved by the Institutional Animal Care and Use Committee (Peking University Shenzhen Hospital). Balb/c-Nude female mice aged 3-5 weeks were purchased from Gempharmatech Co., Ltd. For subcutaneous tumor models,  $3-5 \times 10^6$  tumor cells were suspended in a 100-200  $\mu$ L PBS mixture and then inoculated. Patient-derived xenograft (PDX) models were developed by implanting biopsied human GC tissue into the flanks of 5-week-old female Balb/c-Nude mice.

### Radiolabeling

The procedure for synthesizing <sup>18</sup>F-FAPI-42-RGD was as follows. First, <sup>18</sup>F was produced using a medical cyclotron (MINItrace, GE Healthcare, USA), transferred onto a QMA cartridge (Waters Corporation, USA), followed by elution with 0.5 mL of saline. For radiolabeling, <sup>18</sup>F in saline (50  $\mu$ L, 370-740 MBq) was mixed with 350  $\mu$ L N,N-Dimethylformamide (DMF), 5.0  $\mu$ L glacial acetic acid, and 6.0  $\mu$ L 2.0 mM AlCl<sub>3</sub> for 5 minutes at room temperature to form the [Al<sup>18</sup>F]<sup>2+</sup> conjugate. Next, 50  $\mu$ L of the precursor (1 mg/mL) in highly pure water was introduced to the reaction mixture and heated at 100°C for 10 minutes. Following this, the reaction mixture was diluted with 5 mL of highly pure water and subjected to purification using a Sep-Pak Light C18 cartridge (Waters Corporation, USA). The final product was obtained by eluting the C18 cartridge with 5 mL of saline followed by 1.5 mL of anhydrous ethanol, and then diluting the mixture with 5 mL of 0.9% sterile NaCl solution containing ascorbic acid at a concentration of 10 mg/mL. Radio-HPLC was used to determine the radiochemical purity and stability of <sup>18</sup>F-FAPI-42-RGD.

### Micro-PET imaging and biodistribution in mice bearing xenografts

PET scans using wBIT Micro-PET (Developed by Shenzhen Bay Lab and Bay Imaging Technology Co., Ltd.) were conducted on tumor-xenografted mice (MKN-45, N87-18.2, NUGC4, and GC-PDX) following a tail vein injection of approximately 7.4 MBq of <sup>18</sup>F-FAPI-42-RGD for a 10-min-

**Table 1.** Baseline characteristics of GC patients

Patients (n)	33
Age (years)	
Mean ± SD	62.9 ± 11.0
Gender, n (%)	
Men	24 (72.7)
Women	9 (27.3)
pT-category, n (%)	
pT1	10 (30.3)
pT2	6 (18.2)
pT3	12 (36.4)
pT4	5 (15.2)
pN-category, n (valid %)	
pN0	11 (33.3)
pN1	7 (21.2)
pN2	10 (30.3)
pN3	5 (15.2)
FAP H-score, n (valid %)	
<20	5 (15.2)
≥20	28 (84.8)
Integrin αv H-score, n (valid %)	
<20	26 (78.8)
≥20	7 (21.2)

ute static PET imaging session. The mice were then anesthetized at 1-, 2-, and 4-hours post-injection (p.i.) and positioned in the imaging chamber of the PET scanner for imaging. For comparative purposes, the tumor-bearing mice (n = 3) also received intravenous injections of approximately 7.4 MBq of <sup>18</sup>F-FAPI-42 (Guangdong Gyroscope Pharmaceutical Technology Co., Ltd.) for PET imaging. A blocking study was also conducted on MKN-45 tumor-xenografted mice (n = 3) by first administering unlabeled FAPI-42-RGD before the injection of <sup>18</sup>F-FAPI-42-RGD. PET images were reconstructed using 3D ordered subset expectation maximization (3D OSEM) and manually drawn regions of interest (ROI) using PMOD software (PMOD Technologies LLC, Zurich, Switzerland). The ROI data were then normalized to the administered activity to parameterize images as %ID/g.

Following PET imaging at the final time point, the mice were euthanized. Biological samples, such as blood, liver, kidney, and tumor, were obtained and wet-weighted. The radioactive content of these samples was then measured utilizing an automated γ-counter. Subsequently, the uptake percentage expressed as %ID/g was determined and reported for primary organs or tissues.

#### Statistical analysis

Data analysis was conducted with GraphPad software to perform statistical analyses. The results, presented as mean ± SD, were considered statistically significant when *P*-values <0.05.

## Results

### Patient characteristics

In the cohort, 72.7% (24/33) of the patients were male, with a median age of 64 years. Among all cases, the most common classifications were pT3 (12/33, 36.4%) and pN0 (11/33, 33.3%). FAP was detected in 84.8% of patients with an H-score of 20 or higher. However, in cases with an H-score of 20 or higher, the incidence of integrin αv was only 21.2%. Detailed clinical pathological information for GC patients is presented in **Table 1**.

### FAP and integrin αv IHC staining in GC patients

Representative images of FAP and integrin αv staining are presented in **Figure 1A-F**. No significant differences in FAP expression were observed among GC patients with varying T-staging and N-staging (**Figure 1G, 1H**). In contrast, integrin αv expression in T3 and T4 patients was significantly lower than that in T1 patients (8.8 ± 5.9 vs. 16.8 ± 8.1, *P* = 0.0173 and 7.3 ± 4.4 vs. 16.8 ± 8.1, *P* = 0.0309, respectively) (**Figure 1I**). However, the staining intensity of integrin αv did not show significant differences among GC patients with different N-staging (**Figure 1J**).

### Synthesis, radiochemistry, and stability

The radiolabeling yield was 56.4 ± 4.0% (n = 3). The radiochemical purity of <sup>18</sup>F-FAPI-42-RGD exceeded 98%, as determined by HPLC with a retention time of 13.5 minutes (**Figure 2A**). As illustrated in **Figure 2B**, the radiochemical purity of the probe remained above 98% after incubation in PBS and fetal bovine serum (FBS) at 37 °C for 2 hours.

### Micro-PET imaging and biodistribution in MKN-45 tumor model

For the in vivo biodistribution and targeting efficiency of <sup>18</sup>F-FAPI-42-RGD, we performed micro-PET scanning using both <sup>18</sup>F-FAPI-42-RGD and <sup>18</sup>F-FAPI-42 in GC xenografts in mice and compared the results head-to-head. Micro-PET images of <sup>18</sup>F-FAPI-42-RGD and <sup>18</sup>F-FAPI-42 recorded in the MKN-45 tumor model between 1 to 4 h are presented in **Figure 3A**. The tumor uptake of <sup>18</sup>F-FAPI-42-RGD was significantly higher than normal tissues (**Figure 3A**), with tumor uptake values calculated to be 5.35 ± 0.81, 6.58 ± 1.81, and 6.94 ± 0.51 %ID/g at 1, 2, and 4 h p.i., respectively. In contrast, normal tissue uptakes of <sup>18</sup>F-FAPI-42-RGD were lower than that of the tumor, especially at 4 h p.i. (heart uptake was 4.88 ± 0.60 %ID/g, liver uptake was 3.09 ± 0.11 %ID/g, kidney uptake was 3.03 ± 0.58 %ID/g, and muscle uptake was 1.42 ± 0.34 %ID/g at 4 h) (**Figure 3B**). To evaluate the targeting specificity, unlabeled FAPI-42-RGD was administered 1 h before the injection of <sup>18</sup>F-FAPI-42-RGD. The tumor uptake was greatly inhibited by blocking with unlabeled FAPI-42-RGD in MKN-

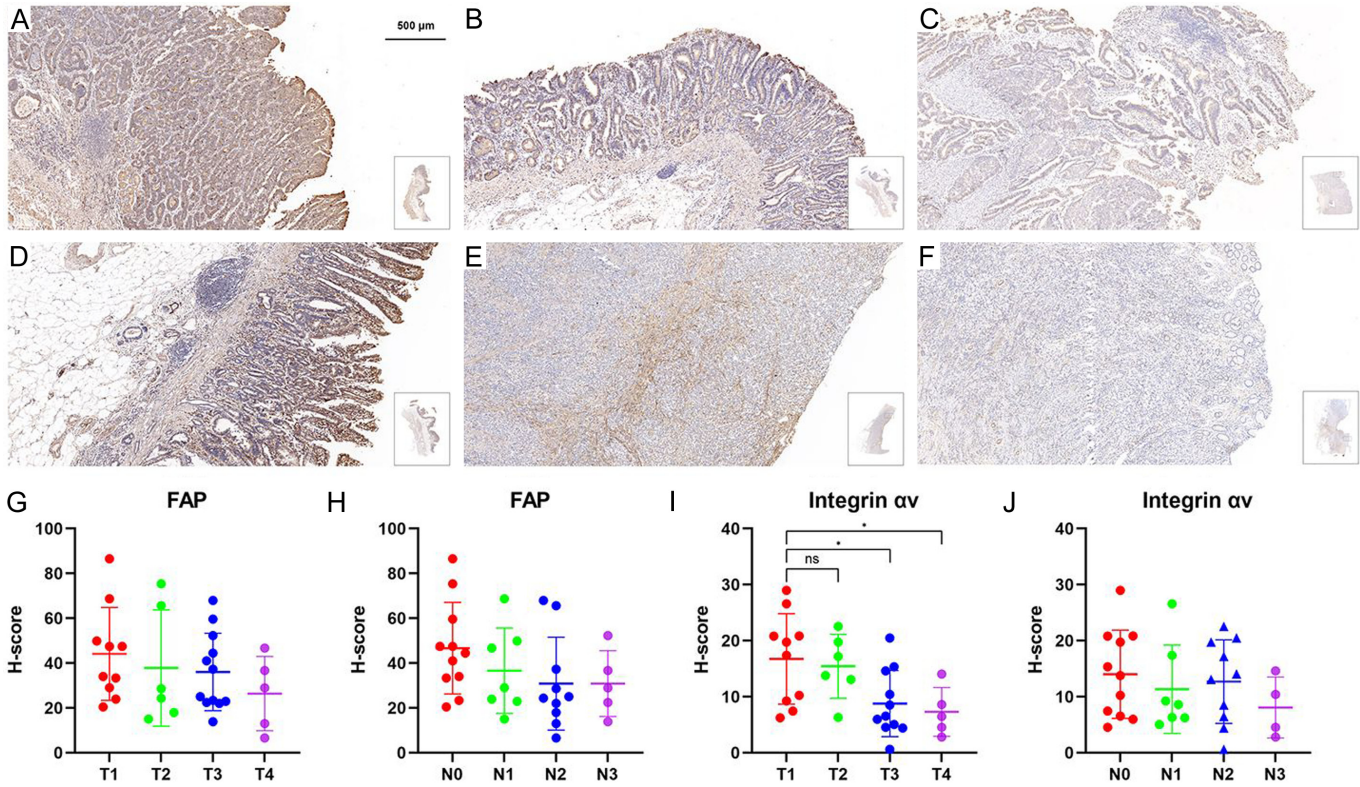


**Figure 1.** Immunohistochemical analysis of FAP and integrin  $\alpha v$  expression in human gastric cancer tissue. (A-C) High (A), medium (B) and low (C) expression of FAP in GC specimens. (D-F) High (D), medium (E) and low (F) expression of integrin  $\alpha v$  in GC specimens. (G, H) The associations of FAP H-score with T-staging (G) and N-staging (H). (I, J) The associations of integrin  $\alpha v$  H-score with T-staging (I) and N-staging (J).

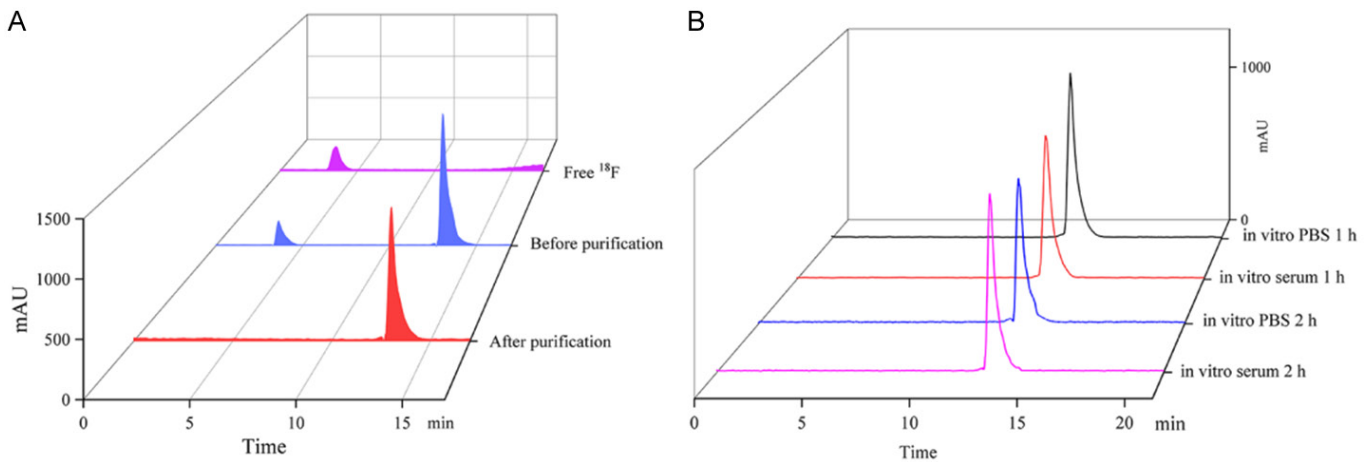


**Figure 2.** Synthesis and in vitro analysis of  $^{18}\text{F}$ -FAP-42-RGD. A: HPLC analysis of  $^{18}\text{F}$ -FAP-42-RGD, demonstrating greater than 98% purity. B: In vitro stability of  $^{18}\text{F}$ -FAP-42-RGD after incubation in PBS or fetal bovine serum at 37  $^{\circ}\text{C}$  for 1 h and 2 h, respectively.

45 xenografts (**Figure 3A, 3C** and **3E**). By contrast, PET imaging of  $^{18}\text{F}$ -FAP-42 (**Figure 3A**) showed that the MKN-45 tumor signal was significantly lower than that of  $^{18}\text{F}$ -FAP-42-RGD. MKN-45 tumor uptake values of  $^{18}\text{F}$ -FAP-42 were  $3.11 \pm 0.83$ ,  $2.94 \pm 0.65$ , and  $2.73 \pm 0.64$  %ID/g at 1, 2, and 4 h p.i., respectively (**Figure 3D** and **3E**).

To further evaluate the pharmacokinetic properties in vivo, biodistribution studies were conducted using MKN-45 tumor-bearing mice (**Figure 3F**). As illustrated in **Figure 3F**, the tumor uptake of  $^{18}\text{F}$ -FAP-42-RGD was measured at  $4.97 \pm 1.36$  %ID/g at 4 h p.i. In contrast, significantly lower tumor uptake was observed in the  $^{18}\text{F}$ -FAP-42-RGD with blocking FAP-42-RGD group and the  $^{18}\text{F}$ -FAP-42

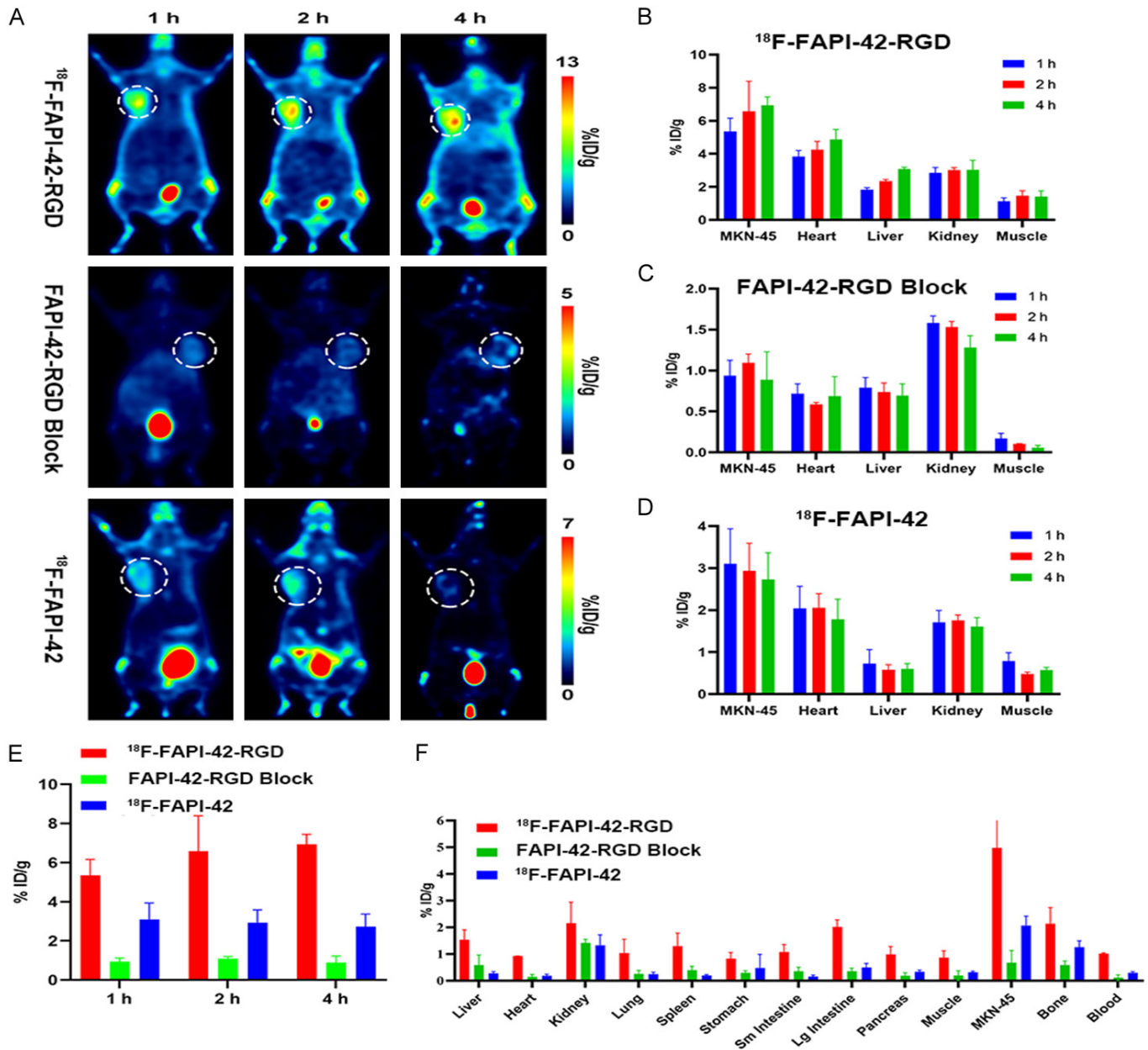


**Figure 3.** <sup>18</sup>F-FAPI-42-RGD and <sup>18</sup>F-FAPI-42 imaging and biodistribution in the MKN-45 xenograft model. (A) Micro-PET imaging of <sup>18</sup>F-FAPI-42-RGD, blocking FAPI-42-RGD+<sup>18</sup>F-FAPI-42-RGD and <sup>18</sup>F-FAPI-42 in MKN-45 subcutaneous xenograft tumor mice at 1, 2, and 4 h p.i. The MKN-45 tumors are indicated by white circles. (B-D) ROI analysis of <sup>18</sup>F-FAPI-42-RGD (B), blocking FAPI-42-RGD+<sup>18</sup>F-FAPI-42-RGD (C) and <sup>18</sup>F-FAPI-42 (D) at different time points. (E) The tumor uptake of PET imaging of <sup>18</sup>F-FAPI-42-RGD, blocking FAPI-42-RGD+<sup>18</sup>F-FAPI-42-RGD and <sup>18</sup>F-FAPI-42 at different time points. (F) Biodistribution data showed uptake of <sup>18</sup>F-FAPI-42-RGD, blocking FAPI-42-RGD+<sup>18</sup>F-FAPI-42-RGD and <sup>18</sup>F-FAPI-42 in the tumor, blood, major organs, and tissues at 4 h.

group, with values of  $0.67 \pm 0.46$  %ID/g and  $2.18 \pm 1.26$  %ID/g, respectively.

*Micro-PET imaging and biodistribution study in N87-18.2 tumor model*

We next studied the imaging of <sup>18</sup>F-FAPI-42-RGD and <sup>18</sup>F-FAPI-42 in N87-18.2 xenograft mice. As shown in **Figure 4A**, the PET image showed that <sup>18</sup>F-FAPI-42-RGD was characterized by rapid tumor uptake and long-term retention in N87-18.2 tumors. In N87-18.2 tumors, higher signal intensity was observed 1 hour after injection and

persisted at later time points. ROI analysis showed that the average uptake of <sup>18</sup>F-FAPI-42-RGD at 1, 2, and 4 h was  $3.11 \pm 1.08$ ,  $5.13 \pm 1.18$ , and  $5.81 \pm 1.84$  %ID/g, respectively (**Figure 4B, 4D**). <sup>18</sup>F-FAPI-42 PET image showed obviously lower tumor uptake compared with that of <sup>18</sup>F-FAPI-42-RGD (**Figure 4A**). The tumor uptake values at 1, 2, and 4 h p.i. were  $2.11 \pm 0.21$ ,  $1.42 \pm 0.25$ , and  $1.43 \pm 0.45$  %ID/g, respectively (**Figure 4C, 4D**).

To enhance the assessment of the in vivo pharmacokinetic characteristics, we conducted biodistribution analyses in mice with N87-18.2 tumors. **Figure 4E** illustrates

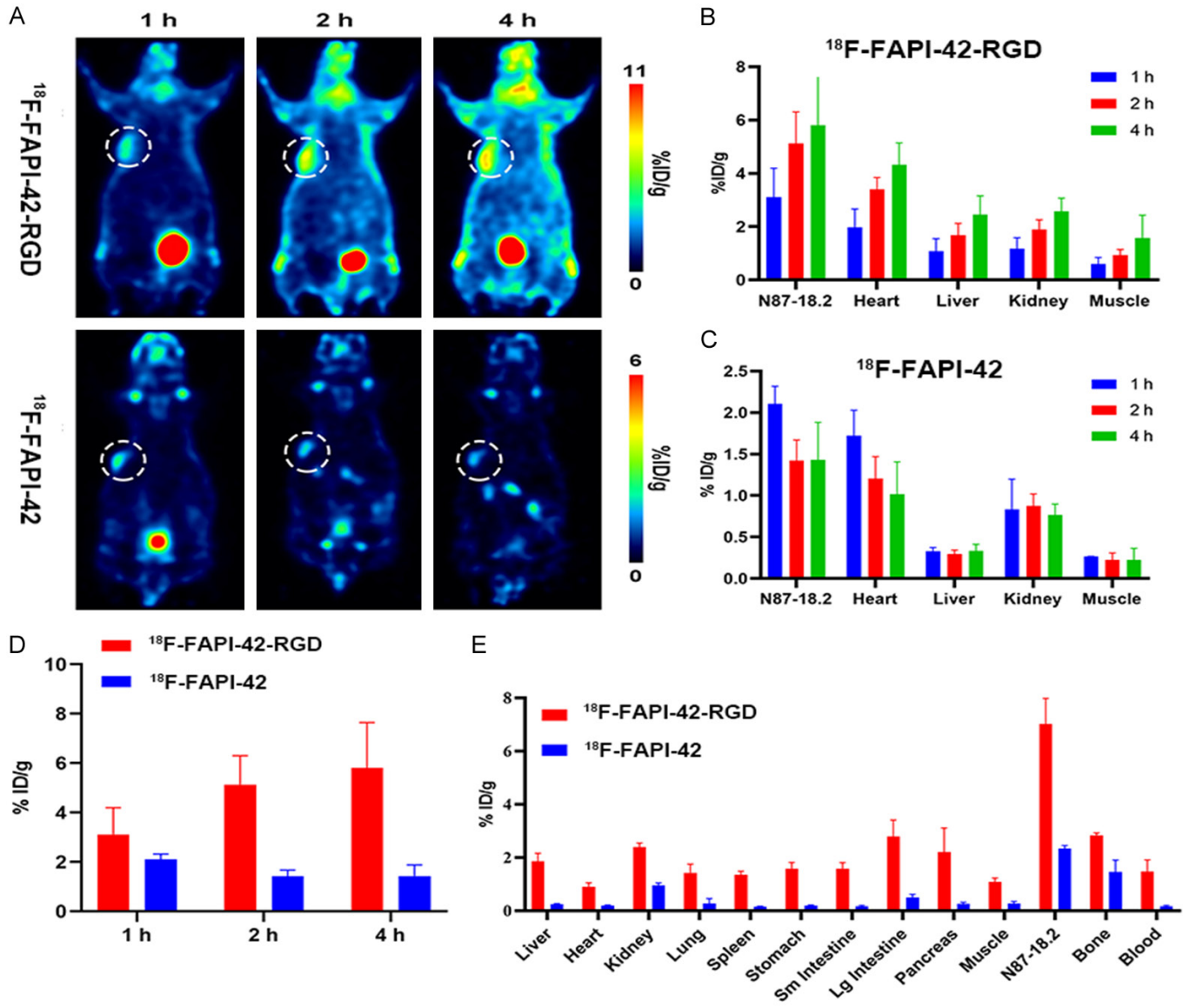


**Figure 4.**  $^{18}\text{F}$ -FAPI-42-RGD and  $^{18}\text{F}$ -FAPI-42 imaging and biodistribution in the N87-18.2 xenograft model. (A) Micro-PET imaging of  $^{18}\text{F}$ -FAPI-42-RGD and  $^{18}\text{F}$ -FAPI-42 in N87-18.2 subcutaneous xenograft tumor mice at 1, 2, and 4 h p.i. The N87-18.2 tumors are indicated by white circles. (B, C) ROI analysis of  $^{18}\text{F}$ -FAPI-42-RGD (B) and  $^{18}\text{F}$ -FAPI-42 (C) at different time points. (D) The tumor uptake of PET imaging of  $^{18}\text{F}$ -FAPI-42-RGD and  $^{18}\text{F}$ -FAPI-42 at different time points. (E) Biodistribution data showed uptake of  $^{18}\text{F}$ -FAPI-42-RGD and  $^{18}\text{F}$ -FAPI-42 in the tumor, blood, major organs, and tissues at 4 h.

that the tumor uptake of  $^{18}\text{F}$ -FAPI-42-RGD at 4 hours following administration is  $7.02 \pm 0.97$  %ID/g. Additionally, we carried out similar biodistribution investigations for  $^{18}\text{F}$ -FAPI-42 in the same tumor model. After 4 hours, the tumor uptake for  $^{18}\text{F}$ -FAPI-42 measured  $2.34 \pm 0.11$  %ID/g, which was notably lower than that of  $^{18}\text{F}$ -FAPI-42-RGD.

#### Micro-PET imaging and biodistribution study in NUGC4 tumor model

Subsequently, we investigated the imaging capabilities of  $^{18}\text{F}$ -FAPI-42-RGD and  $^{18}\text{F}$ -FAPI-42 in mice with NUGC4 xenografts. As illustrated in **Figure 5A**, PET imaging revealed that  $^{18}\text{F}$ -FAPI-42-RGD exhibited rapid uptake and

prolonged retention in NUGC4 tumors. Notably, at just 1 h p.i., enhanced signal intensity was detected in NUGC4 tumors, which persisted consistently at the later time points. The ROI analysis indicated that the average uptake of  $^{18}\text{F}$ -FAPI-42-RGD was recorded as  $2.15 \pm 0.51$  %ID/g,  $2.62 \pm 0.09$ , and  $3.06 \pm 0.22$  %ID/g at 1, 2, and 4 h p.i., respectively (**Figure 5B, 5D**). In contrast, imaging data for  $^{18}\text{F}$ -FAPI-42, presented in **Figure 5A**, yielded tumor uptake values of  $1.86 \pm 0.44$ ,  $2.22 \pm 0.14$ , and  $2.32 \pm 0.10$  %ID/g at 1, 2, and 4 h p.i., respectively (**Figure 5C, 5D**), which was slightly lower than that of  $^{18}\text{F}$ -FAPI-42-RGD.

We also carried out biodistribution studies in mice bearing NUGC4 tumors. As shown in **Figure 5E**, the uptake of  $^{18}\text{F}$ -FAPI-42-RGD was determined to be  $3.03 \pm 0.59$  %ID/g

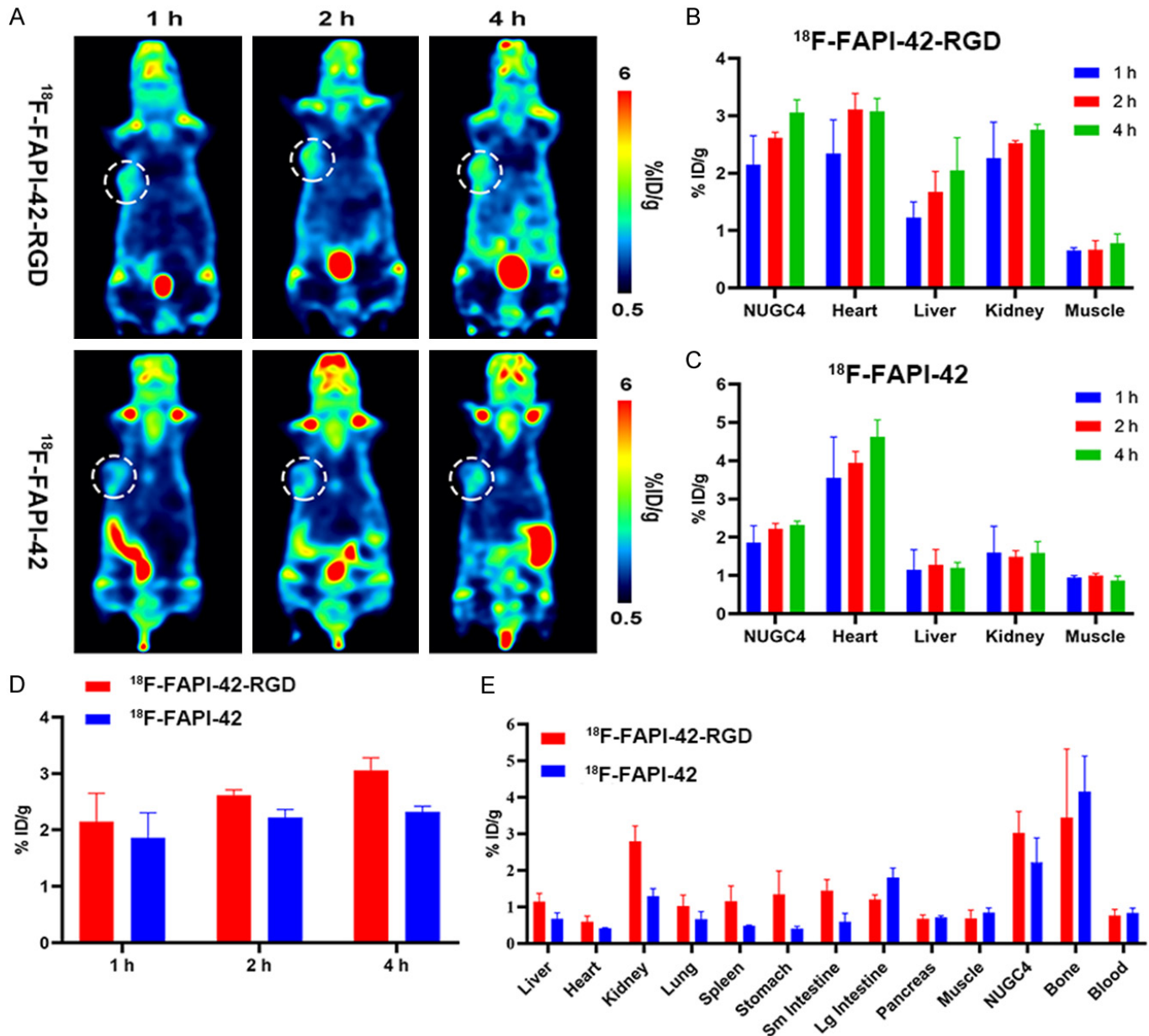


**Figure 5.**  $^{18}\text{F}$ -FAPI-42-RGD and  $^{18}\text{F}$ -FAPI-42 imaging and biodistribution in the NUGC4 xenograft model. (A) Micro-PET imaging of  $^{18}\text{F}$ -FAPI-42-RGD and  $^{18}\text{F}$ -FAPI-42 in NUGC4 subcutaneous xenograft tumor mice at 1, 2, and 4 h p.i. The NUGC4 tumors are indicated by white circles. (B, C) ROI analysis of  $^{18}\text{F}$ -FAPI-42-RGD (B) and  $^{18}\text{F}$ -FAPI-42 (C) at different time points. (D) The tumor uptake of PET imaging of  $^{18}\text{F}$ -FAPI-42-RGD and  $^{18}\text{F}$ -FAPI-42 at different time points. (E) Biodistribution data showed uptake of  $^{18}\text{F}$ -FAPI-42-RGD and  $^{18}\text{F}$ -FAPI-42 in the tumor, blood, major organs, and tissues at 4 h.

at the 4-hour after injection. At this same time point, the tumor uptake recorded for  $^{18}\text{F}$ -FAPI-42 was  $2.22 \pm 0.67$  %ID/g, which was considerably lower compared to the uptake seen with  $^{18}\text{F}$ -FAPI-42-RGD.

#### Micro-PET imaging and biodistribution study in GC-PDX tumor model

In this study, we investigated the imaging of GC-PDX tumor-bearing mice using  $^{18}\text{F}$ -FAPI-42-RGD and  $^{18}\text{F}$ -FAPI-42. As illustrated in **Figure 6A**, the PET images indicated that  $^{18}\text{F}$ -FAPI-42-RGD rapidly accumulated in the tumor and demonstrated significant retention within the GC-PDX

tumor. Notably, the signal intensity in the GC-PDX tumor increased one hour p.i. and remained elevated over time. The Region of Interest (ROI) analysis quantified the mean uptake of  $^{18}\text{F}$ -FAPI-42-RGD at 1, 2, and 4 h p.i. as  $3.93 \pm 1.35$ ,  $4.42 \pm 1.96$ , and  $4.69 \pm 0.97$  %ID/g, respectively (**Figure 6B, 6D**). In stark contrast, the uptake of  $^{18}\text{F}$ -FAPI-42 remained consistently low throughout the assessment period, with values of  $1.72 \pm 0.21$ ,  $1.39 \pm 0.16$ , and  $1.10 \pm 0.06$  %ID/g at 1, 2, and 4 h p.i., respectively (**Figure 6C, 6D**).

Following the final imaging session at the 4-hour mark, all major organs were harvested for gamma counting (**Figure**

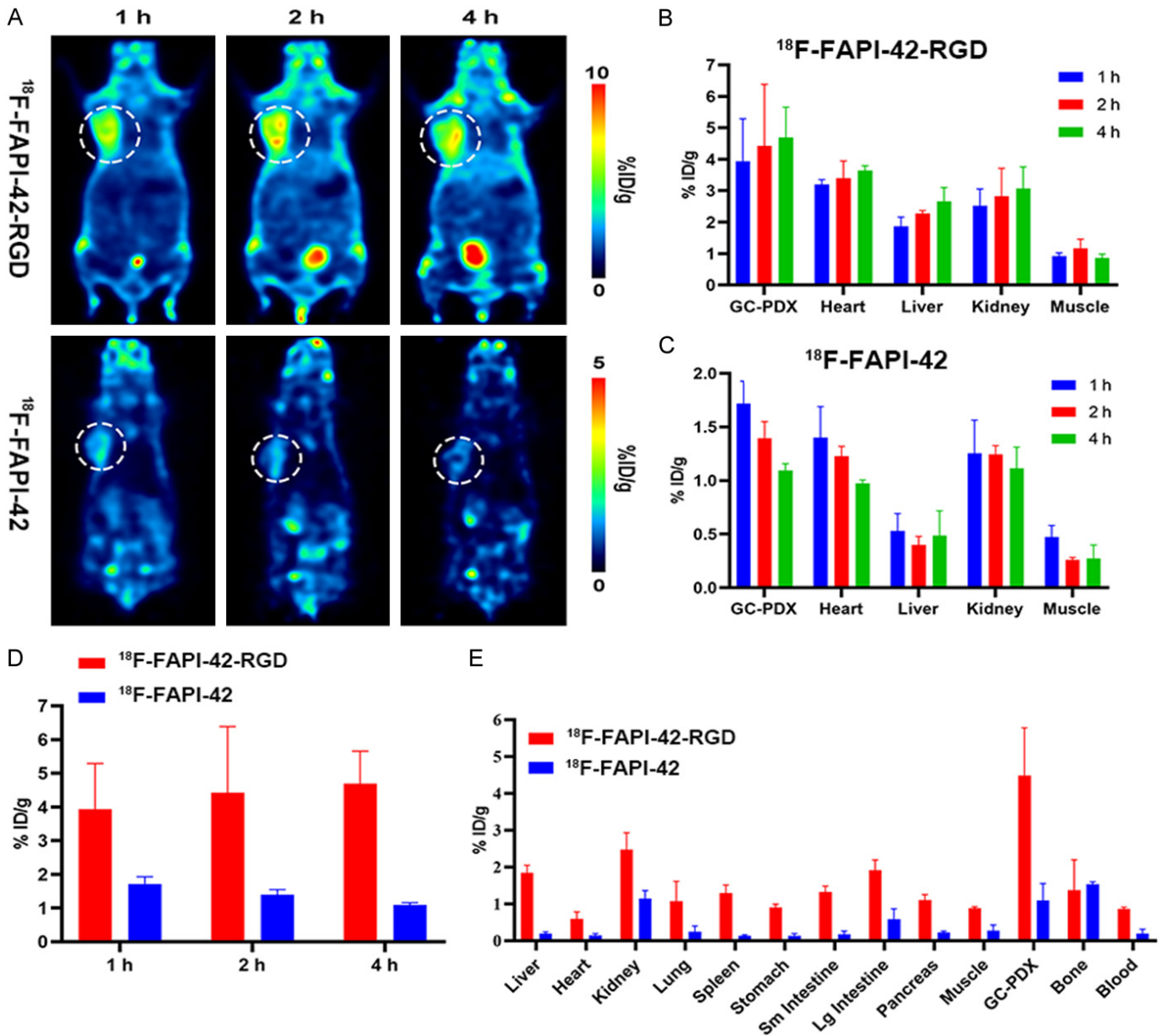


**Figure 6.** <sup>18</sup>F-FAPI-42-RGD and <sup>18</sup>F-FAPI-42 imaging and biodistribution in the GC-PDX xenograft model. (A) Micro-PET imaging of <sup>18</sup>F-FAPI-42-RGD and <sup>18</sup>F-FAPI-42 in GC-PDX subcutaneous xenograft tumor mice at 1, 2, and 4 h p.i. The GC-PDX tumors are indicated by white circles. (B, C) ROI analysis of <sup>18</sup>F-FAPI-42-RGD (B) and <sup>18</sup>F-FAPI-42 (C) at different time points. (D) The tumor uptake of PET imaging of <sup>18</sup>F-FAPI-42-RGD and <sup>18</sup>F-FAPI-42 at different time points. (E) Biodistribution data showed uptake of <sup>18</sup>F-FAPI-42-RGD and <sup>18</sup>F-FAPI-42 in the tumor, blood, major organs, and tissues at 4 h.

**6E).** Consistent with the ROI findings, the accumulation of <sup>18</sup>F-FAPI-42-RGD in the GC-PDX tumors was significantly greater compared to that of <sup>18</sup>F-FAPI-42, with values of  $4.49 \pm 1.29$  %ID/g versus  $1.09 \pm 0.46$  %ID/g.

**Discussion**

This study preliminarily revealed the expression of FAP and integrin  $\alpha_v$  in human GC tissues. Our findings indicated that over 80% of GC patients exhibited high expression levels of FAP, while more than 20% demonstrated elevated expression of integrin  $\alpha_v$ . Lyu et al. have confirmed that FAP serves as a novel biomarker for GC and significantly influences the poor prognosis associated

with this disease [22]. Additionally, Wu et al. found that integrin  $\alpha_v$  was significantly more prevalent in GC tissues compared to normal tissues [23]. The evidence indicates that FAP and integrin  $\alpha_v$  may significantly contribute to the progression of GC. Our study revealed that the expression levels of integrin  $\alpha_v$  were higher in patients diagnosed with T1 GC compared to those with T3 and T4 stages. However, we did not observe any significant differences in FAP expression across the various T and N stages. This inconsistency may be due to the limited sample size in our investigation.

In recent years, numerous studies have demonstrated that FAPs PET imaging can be utilized for the diagnosis of

GC [24, 25]. However, it is important to note that the sensitivity of <sup>68</sup>Ga-FAPI is limited in the early detection of GC in the mucosa and submucosa, with only 37.5% of primary lesions exhibiting the high sensitivity of <sup>68</sup>Ga-FAPI [26]. Recent research has shown that homodimeric radiotracers enhance tumor uptake and retention compared to previously developed monomeric radiotracers [20]. The RGD peptide sequence exhibits a high affinity and selectivity for integrin  $\alpha\beta3$ , making it an ideal candidate for the development of various PET formulations [27]. FAP and integrin  $\alpha\nu$  are two proteins that are highly expressed in human GC tissues. Notably, the expression of integrin  $\alpha\nu$  at the T1 stage of GC is higher than that observed in the T3 and T4 stages. This suggests that the PET probe targeting integrin  $\alpha\nu$  may demonstrate greater sensitivity in the detection of early-stage GC. Two studies have investigated the application of dual-specific radiotracers, <sup>18</sup>F-FAPI-02-RGD and <sup>68</sup>Ga-FAPI-02-RGD, in various tumor models and clinical patients. The findings indicated that the tumor uptake of these dual-specific radiotracers surpassed that of <sup>18</sup>F-FAPI-02 and <sup>68</sup>Ga-FAPI-02, respectively [18, 20]. Additionally, <sup>18</sup>F-FAPI-42 exhibited excellent imaging and detection capabilities in tumors with high FAP expression [25]. Currently, there are no studies on <sup>18</sup>F-FAPI-42-RGD. Consequently, we designed and developed a dual-specific heterodimeric radiotracer, <sup>18</sup>F-FAPI-42-RGD, which targets FAP and  $\alpha\beta3$  for <sup>18</sup>F-based PET imaging in GC.

In our study, the <sup>18</sup>F-FAPI-42-RGD labeling method demonstrated high purity and radiochemical efficiency. Given that free <sup>18</sup>F specifically binds to bone, the stability of the label is a significant concern. Stability testing revealed that <sup>18</sup>F-FAPI-42-RGD remained intact after a 2-hour incubation with FBS or PBS, indicating that this labeling method was both effective and suitable for high yield. Additionally, Liu et al. reported that <sup>18</sup>F-FAPI-02-RGD exhibited good stability over a 2-hour period [18]. These findings suggest that the stability of <sup>18</sup>F-FAPI-42-RGD in our study is comparable to that previously reported.

To highlight the key distinguishing features of FAPI-42-RGD, we compared the dual-target probe <sup>18</sup>F-FAPI-42-RGD with the single-target probe <sup>18</sup>F-FAPI-42 in various GC models. These models included xenografts derived from GC cell lines (MKN-45, N87-18.2, and NUGC4) as well as a GC-PDX model. Compared to <sup>18</sup>F-FAPI-42, the MKN-45 tumor uptake and retention of <sup>18</sup>F-FAPI-42-RGD were significantly enhanced at all examined time points. Furthermore, <sup>18</sup>F-FAPI-42-RGD exhibited higher uptake than <sup>18</sup>F-FAPI-42 in normal organs. In other tumor models, including N87-18.2, NUGC4, and GC-PDX, <sup>18</sup>F-FAPI-42-RGD exhibited comparable performance. In blocking experiments, non-radioactively labeled FAPI-42-RGD demonstrated significant inhibition of <sup>18</sup>F-FAPI-42-RGD uptake in MKN-45 tumors, thereby confirming the specificity of the designed tracer. Tumor uptake in different models of GC is not the same, which may be related to the expression levels of FAP and integrin  $\alpha\beta3$  in the tumor.

Moreover, the visualization of <sup>18</sup>F-FAPI-42-RGD absorption in the tumor was observed at 1 h, while all non-target organs exhibited low uptake. This resulted in a consistently high tumor-to-background ratio. Liu et al. confirmed that the tumor uptake of <sup>18</sup>F-FAPI-02-RGD was greater than that of most normal organs, including the kidneys, at each time point within a 4-hour period [18]. Our analysis of <sup>18</sup>F-FAPI-42-RGD PET data and biodistribution yielded comparable results. Chen et al. evaluated the clinical feasibility of <sup>68</sup>Ga-FAPI-RGD PET for imaging of various types of cancer and the dual-targeting tracer showed improved tumor uptake and TBR compared with <sup>68</sup>Ga-FAPI [19]. The great clinical translation potential of dual-targeting PET radiotracers that target both FAP and integrin  $\alpha\beta3$  receptors in cancer patients has been indicated in many studies [17-19, 28, 29]. Based on the above previous studies, we will also perform the clinical study of <sup>18</sup>F-FAPI-42-RGD in GC patients in future to explore its great clinical translation potential for diagnosing gastric cancer. FAP is recognized as a valuable target for both imaging and treatment of tumors. Numerous studies have indicated that FAPI multimers labeled with <sup>177</sup>Lu and <sup>225</sup>Ac exhibit significant therapeutic promise [30-32]. Consequently, we propose that FAPI-42-RGD after chemical optimization, labeled with <sup>177</sup>Lu and <sup>225</sup>Ac, could serve as promising therapeutic radiopharmaceuticals. Future research will investigate the therapeutic potential of chemically optimized FAPI-42-RGD.

This study presents a novel dual-targeting tracer, <sup>18</sup>F-FAPI-42-RGD, which targets both FAP and integrin  $\alpha\beta3$ . However, it is important to note certain limitations. Cell-binding assay was not conducted to indicate the binding affinity of FAPI-42-RGD for FAP and integrin  $\alpha\beta3$ . But we demonstrated that FAPI-42-RGD exhibited superior tumor binding ability in various GC tumor models compared with that of FAPI-42. While preclinical evaluations included a head-to-head comparison with <sup>18</sup>F-FAPI-42, future studies should also conduct head-to-head comparisons with <sup>18</sup>F-FAPI-42-RGD. The expression levels of FAP and RGD in tumor-xenografted mice (MKN-45, N87-18.2, NUGC4, and GC-PDX) should be verified in our future research.

While preclinical evaluations have been conducted in select GC models, future PET imaging comparisons should specifically focus on distinct types of GC models, including FAP-/ $\alpha\beta3$ + GC models, FAP+/ $\alpha\beta3$ - GC models, and FAP+/ $\alpha\beta3$ + GC models, to demonstrate the advantages of dual targeting.

## Conclusion

In this study, we reported the synthesis of a novel FAPI-RGD heterodimer, <sup>18</sup>F-FAPI-42-RGD, and investigated its pharmacokinetics and efficacy in GC tumor models. The <sup>18</sup>F-FAPI-42-RGD compound demonstrated higher tumor uptake compared to <sup>18</sup>F-FAPI-42, leading to enhanced tumor-background contrast. Our present study suggested that <sup>18</sup>F-FAPI-42-RGD holds significant potential for clinical

cal applications in the imaging and diagnosis of gastric cancer. Further studies are warranted to explore its clinical utility and validate its efficacy in human patients.

## Acknowledgements

We all thank the patients participated in this study.

## Disclosure of conflict of interest

None.

**Address correspondence to:** Dr. Yongqiang Yu, Department of Radiology, The First Affiliated Hospital of Anhui Medical University, No. 218, Jixi Road, Hefei 230022, Anhui, China. Tel: +86-13923456759; E-mail: yuyongqiang@ahmu.edu.cn

## References

- [1] Sung H, Ferlay J, Siegel RL, Laversanne M, Soerjomataram I, Jemal A and Bray F. Global cancer statistics 2020: GLOBOCAN estimates of incidence and mortality worldwide for 36 cancers in 185 countries. *CA Cancer J Clin* 2021; 71: 209-249.
- [2] Wang Y, Luo W and Li Y. [(68)Ga]Ga-FAPI-04 PET MRI/CT in the evaluation of gastric carcinomas compared with [(18)F]-FDG PET MRI/CT: a meta-analysis. *Eur J Med Res* 2023; 28: 34.
- [3] Jayaprakasam VS, Paroder V and Schoder H. Variants and pitfalls in PET/CT imaging of gastrointestinal cancers. *Semin Nucl Med* 2021; 51: 485-501.
- [4] Kalluri R. The biology and function of fibroblasts in cancer. *Nat Rev Cancer* 2016; 16: 582-598.
- [5] Nurmik M, Ullmann P, Rodriguez F, Haan S and Letellier E. In search of definitions: cancer-associated fibroblasts and their markers. *Int J Cancer* 2020; 146: 895-905.
- [6] Loktev A, Lindner T, Burger EM, Altmann A, Giesel F, Kratochwil C, Debus J, Marme F, Jager D, Mier W and Haberkorn U. Development of fibroblast activation protein-targeted radiotracers with improved tumor retention. *J Nucl Med* 2019; 60: 1421-1429.
- [7] Wu F, Yang J, Liu J, Wang Y, Mu J, Zeng Q, Deng S and Zhou H. Signaling pathways in cancer-associated fibroblasts and targeted therapy for cancer. *Signal Transduct Target Ther* 2021; 6: 218.
- [8] Mori Y, Dendl K, Cardinale J, Kratochwil C, Giesel FL and Haberkorn U. FAPI PET: fibroblast activation protein inhibitor use in oncologic and nononcologic disease. *Radiology* 2023; 306: e220749.
- [9] Baum RP, Schuchardt C, Singh A, Chantadisai M, Robiller FC, Zhang J, Mueller D, Eismant A, Almaguel F, Zboralski D, Osterkamp F, Hoehne A, Reineke U, Smerling C and Kulkarni HR. Feasibility, biodistribution, and preliminary dosimetry in peptide-targeted radionuclide therapy of diverse adenocarcinomas using (177)Lu-FAP-2286: first-in-humans results. *J Nucl Med* 2022; 63: 415-423.
- [10] Pang Y, Zhao L, Meng T, Xu W, Lin Q, Wu H, Zhang J, Chen X, Sun L and Chen H. PET imaging of fibroblast activation protein in various types of cancer using (68)Ga-FAP-2286: comparison with (18)F-FDG and (68)Ga-FAPI-46 in a single-center, prospective study. *J Nucl Med* 2023; 64: 386-394.
- [11] Promteangtrong C, Siripongsatian D, Jantarato A, Kunawudhi A, Kiatkittikul P, Yaset S, Boonkawin N and Chotipanich C. Head-to-head comparison of (68)Ga-FAPI-46 and (18)F-FDG PET/CT for evaluation of head and neck squamous cell carcinoma: a single-center exploratory study. *J Nucl Med* 2022; 63: 1155-1161.
- [12] Desgrosellier JS and Cheresh DA. Integrins in cancer: biological implications and therapeutic opportunities. *Nat Rev Cancer* 2010; 10: 9-22.
- [13] Li L, Zheng J, Liu Z, Huang Y, Xiao J, Wang S, Yu Q, Zhang Q, Hu X, Zhao W, Hou W, Spring KF, Yu J and Yuan S. Pre-treatment (18)F-RGD uptake may predict adverse events during apatinib antiangiogenic therapy. *Clin Oncol (R Coll Radiol)* 2022; 34: e238-e245.
- [14] Chen H, Niu G, Wu H and Chen X. Clinical application of radiolabeled RGD peptides for PET imaging of integrin  $\alpha$ v $\beta$ 3. *Theranostics* 2016; 6: 78-92.
- [15] Eder M, Schafer M, Bauder-Wust U, Haberkorn U, Eisenhut M and Kopka K. Preclinical evaluation of a bispecific low-molecular heterodimer targeting both PSMA and GRPR for improved PET imaging and therapy of prostate cancer. *Prostate* 2014; 74: 659-668.
- [16] Liu Z, Niu G, Wang F and Chen X. (68)Ga-labeled NOTA-RGD-BBN peptide for dual integrin and GRPR-targeted tumor imaging. *Eur J Nucl Med Mol Imaging* 2009; 36: 1483-1494.
- [17] Wang R, Jakobsson V, Wang J, Zhao T, Peng X, Li B, Xue J, Liang N, Zhu Z, Chen X and Zhang J. Dual targeting PET tracer [(68)Ga]Ga-FAPI-RGD in patients with lung neoplasms: a pilot exploratory study. *Theranostics* 2023; 13: 2979-2992.
- [18] Liu N, Wan Q, Wu X, Zhao T, Jakobsson V, Yuan H, Chen X, Zhang J and Zhang W. A comparison of [(18)F]AIF- and (68)Ga-labeled dual targeting heterodimer FAPI-RGD in malignant tumor: preclinical evaluation and pilot clinical PET/CT imaging. *Eur J Nucl Med Mol Imaging* 2024; 51: 1685-1697.
- [19] Zhao L, Wen X, Xu W, Pang Y, Sun L, Wu X, Xu P, Zhang J, Guo Z, Lin Q, Chen X and Chen H. Clinical Evaluation of (68)Ga-FAPI-RGD for imaging of fibroblast activation protein and integrin  $\alpha$ (v) $\beta$ (3) in various cancer types. *J Nucl Med* 2023; 64: 1210-1217.
- [20] Zang J, Wen X, Lin R, Zeng X, Wang C, Shi M, Zeng X, Zhang J, Wu X, Zhang X, Miao W, Xu P, Guo Z, Zhang J and Chen X. Synthesis, preclinical evaluation and radiation dosimetry of a dual targeting PET tracer [(68)Ga]Ga-FAPI-RGD. *Theranostics* 2022; 12: 7180-7190.
- [21] Imam R, Chang Q, Black M, Yu C and Cao W. CD47 expression and CD163(+) macrophages correlated with prognosis of pancreatic neuroendocrine tumor. *BMC Cancer* 2021; 21: 320.
- [22] Lyu Z, Li Y, Zhu D, Wu S, Hu F, Zhang Y, Li Y and Hou T. Fibroblast activation protein- $\alpha$  is a prognostic biomarker associated with ferroptosis in stomach adenocarcinoma. *Front Cell Dev Biol* 2022; 10: 859999.
- [23] Wu S, Nasser B, Singab A, Lin G, Wang Y, Zhu H, Yang G, Chen J, Li J, Li P, Zhao D, Tian J and Ye L. The regulatory role of integrin in gastric cancer tumor microenvironment and drug resistance. *Prog Biophys Mol Biol* 2025; 195: 130-136.

- [24] Yang T, Peng L, Qiu J, He X, Zhang D, Wu R, Liu J, Zhang X and Zha Z. A radiohybrid theranostics ligand labeled with fluorine-18 and lutetium-177 for fibroblast activation protein-targeted imaging and radionuclide therapy. *Eur J Nucl Med Mol Imaging* 2023; 50: 2331-2341.
- [25] Wang S, Zhou X, Xu X, Ding J, Liu S, Hou X, Li N, Zhu H and Yang Z. Clinical translational evaluation of Al(18)F-NOTA-FAPI for fibroblast activation protein-targeted tumour imaging. *Eur J Nucl Med Mol Imaging* 2021; 48: 4259-4271.
- [26] Miao Y, Feng R, Guo R, Huang X, Hai W, Li J, Yu T, Qu Q, Zhang M, Shangguan C, Mi J, Zhu Z and Li B. Utility of [(68)Ga]FAPI-04 and [(18)F]FDG dual-tracer PET/CT in the initial evaluation of gastric cancer. *Eur Radiol* 2023; 33: 4355-4366.
- [27] Li H, Peng W, Zhen Z, Zhang W, Liao S, Wu X, Wang L, Xuan A, Gao Y and Xu J. Integrin alpha(v)beta(3) and EGFR dual-targeted [(64)Cu]Cu-NOTA-RGD-GE11 heterodimer for PET imaging in pancreatic cancer mouse model. *Nucl Med Biol* 2023; 124-125: 108364.
- [28] Chen Y, Zheng S, Zang J, Shao Z, Tu D, Liu Q, Chen X, Miao W and Zhang J. [(68)Ga]Ga-LNC1007 versus 2-[(18)F]FDG in the evaluation of patients with metastatic differentiated thyroid cancer: a head-to-head comparative study. *Eur J Nucl Med Mol Imaging* 2025; 52: 683-692.
- [29] Gao H, Chen J, Yang Z, Zhu Z, He L, Zhang W, Chen X and Zhang J. Comparative study of [(18)F]AIF-LNC1007, [(18)F]FDG, and [(18)F]AIF-NOTA-FAPI-04 PET/CT in breast cancer diagnosis: a methodological exploration and analytical insight. *ACS Appl Mater Interfaces* 2024; 16: 67523-67531.
- [30] Pang Y, Zhao L, Fang J, Chen J, Meng L, Sun L, Wu H, Guo Z, Lin Q and Chen H. Development of FAPI tetramers to improve tumor uptake and efficacy of FAPI radioligand therapy. *J Nucl Med* 2023; 64: 1449-1455.
- [31] Liu Y, Watabe T, Kaneda-Nakashima K, Shirakami Y, Naka S, Ooe K, Toyoshima A, Nagata K, Haberkorn U, Kratochwil C, Shinohara A, Hatazawa J and Giesel F. Fibroblast activation protein targeted therapy using [(177)Lu]FAPI-46 compared with [(225)Ac]FAPI-46 in a pancreatic cancer model. *Eur J Nucl Med Mol Imaging* 2022; 49: 871-880.
- [32] Fu H, Huang J, Zhao T, Wang H, Chen Y, Xu W, Pang Y, Guo W, Sun L, Wu H, Xu P, Su B, Zhang J, Chen X and Chen H. Fibroblast activation protein-targeted radioligand therapy with <sup>177</sup>Lu-EB-FAPI for metastatic radioiodine-refractory thyroid cancer: first-in-human, dose-escalation study. *Clin Cancer Res* 2023; 29: 4740-4750.